

Modal Geometry Governs Proteoform Dynamics

James N. Cobley

The University of Dundee, Dundee, Scotland, UK.

Correspondence: jcobley001@dundee.ac.uk or j_cobley@yahoo.com

Abstract

A central mystery is how a specific proteoform—a distinct molecular variant of a protein—dynamically shapes its own future by evolving into new modes that exist only in potential until realised. Here, Modal Geometric Field (MGF) Theory couples real and abstract proteoform transitions through four axioms. Axioms 1–3 (invariant) dictate that only first-order transitions occur on the discrete, volume-invariant, non-symplectic modal manifold. Axiom 4 (mutable) functorially projects the general relativity–derived curvature of an instantiated proteoform into this modal manifold, coupling what is real to what is abstract. Curvature, conserved per a discrete Noether theorem, actively shapes proteoform dynamics. Because curvature distribution renders activation energy relative, curvature-derived barriers are mutable, in direct analogy to Einstein’s theory. Entropy then emerges inevitably from curvature transport. This unification of energy, entropy, and curvature yields hysteresis, path dependence, fractal self-similarity, and trajectories that oscillate between order and chaos. As a scale-invariant and universal framework, MGF Theory reveals how modal geometry governs proteoform dynamics.

Key words: Modal Geometry, Proteoform, Curvature, Dynamics, Fractal.

Introduction

The real physical geometry of a protein molecule—the structure of a specific biochemical mode (state)—defines both its biological identity and function¹. Discrete molecular shapes arising from mutations, splice variants, or post-translational modifications (PTMs) establish distinct molecular realities: proteoforms^{2–6}. Proteoform dynamics—modal transitions—underpin virtually every biological process³. These transitions inherently involve both what exists now—the instantiated proteoform mode—and what could exist—abstract modes⁷. This necessarily demands a formal mathematical coupling between real and abstract modes.

Statistical mechanics offers the closest approximation⁸. It interprets thermodynamic quantities like activation energy as emergent from probability distributions over microstates—linking what is to what could be. Yet this framework assumes a flat, undifferentiated state space: all configurations are equipotential prior to Boltzmann weighting. No geometric structure guides transitions; no curvature deforms the landscape to favour one path over another. The possibility space is merely enumerated, not shaped. What is missing is a field theory in which the real proteoform sculpts the geometry of its own potential futures.

This work introduces Modal Geometric Field (MGF) Theory, a scale-invariant, universal physical basis of proteoform dynamics. Inspired by general relativity⁹, the mass-energy of an irreducibly real proteoform curves the abstract manifold of possible modes. As demonstrated using cysteine proteoforms^{10,11}, curvature constrains modal transitions. Because curvature distribution renders activation energy relative, curvature-derived barriers are mutable, in direct analogy to Einstein’s theory. Entropy then emerges inevitably from curvature transport. This unification of energy, entropy, and curvature yields hysteresis, path dependence, fractal self-similarity, and trajectories that oscillate between order and chaos.

Results

Axiom 1. Binomial Theorem Structures the Modal Manifold

In the binary basis, each cysteine residue is either reduced (0) or oxidised (1)⁷. Per combinatorics¹², the modal manifold— \mathcal{M} —for a protein with R cysteines is

$$\mathcal{M} = \{0,1\}^R$$

a Boolean lattice (**Figure 1A**) of cardinality

$$|\mathcal{M}| = 2^R$$

Each stratum (\mathbb{S}_k) contains modes of exactly k oxidised cysteine residues, of cardinality

$$|\mathbb{S}_k| = \binom{R}{k}$$

Binomial theorem structures the \mathcal{M} , with the integer of each strata matching the binomial coefficients enumerated in Pascals triangle.

Example: For one of >1,000 human proteins with three cysteine residues⁷ like [GAPDH](#):

$$|\mathcal{M}, (GAPDH)| = 2^3 = 8, (|k_0|, |k_1|, |k_2|, |k_3|) = 1, 3, 3, 1.$$

Concretely,

$$k_0 = 000, k_1 = 100, 010, 001, k_2 = 110, 011, 101, k_3 = 111$$

Axiom 1 applies to any R integer, and naturally extends to a multinomial lattice, accommodating multiple PTMs from sulfenic acids to disulfide bonds¹³. The multinomial theorem extends axiom 1 to the full proteoform universe (**Supplementary Information**).

Axiom 2. Volume-invariance—Discrete Liouville’s Theorem Analogue.

Since the \mathcal{M} enumerates every mode, each molecule must occupy exactly one mode at a time. The total volume—either the number of modes or the probability of mass between them—is conserved. Modes cannot be created or destroyed. Hence, Liouville’s theorem extends to the discrete non-symplectic \mathcal{M} as a conservation law

$$\frac{d}{dt} \sum_{x \in \mathcal{M}} \rho(x) = 0$$

Equivalently, if (P_x) denotes the normalised probability distribution over modes:

$$\frac{d}{dt} \sum_{x \in \mathcal{M}} P(x) = 0$$

For discrete modal transitions with rates k_{xy} between neighbouring modes x and y , conservation is enforced by a discrete continuity equation:

$$\dot{\rho}(x) = \sum_{y \in N(x)} [\rho(y)k_{yx} - \rho(x)k_{xy}], \sum_x \dot{\rho}(x) = 0$$

No matter how molecules redistribute within the manifold, the total mass—viewed as combinatorial volume or probability density—remains invariant (**Figure 1B**). At each timestep, occupancy redistributes across \mathcal{M} , but the total volume is preserved. This is enforced by a discrete continuity equation on the Boolean graph. This is the discrete, non-symplectic analogue of Liouville’s theorem (**Supplementary Information**).

Axiom 3. Conservation of Unitary Mass Ensures All Modal Transitions are First-order

An instantiated mode is a classical object with conserved mass-energy (M). Per axiom 2, molecular occupancy $\rho(x)$ must equal one at the occupied mode and zero elsewhere:

$$\rho(x) = \begin{cases} 1, & x = x_i \\ 0, & \text{otherwise} \end{cases}$$

Discrete modal transitions between nonadjacent modes (e.g., $000 \rightarrow 011$) are forbidden because the fractional transport of unit mass is undefined for classical objects: they have definite position. By definition, their position cannot be in a superimposition of discrete modes. Hence, the only allowed transitions are first-order moves (e.g., $000 \rightarrow 010$) between adjacent modes in the Hamming space of \mathcal{M} .

Formally, nonzero transition probabilities $P(x \rightarrow y)$ must satisfy

$$\text{Hamming}(x, y) = 1$$

The allowed outflow from any mode forms a probabilistic simplex:

$$\sum_{y: \text{Ham}(x,y)=1} P(x \rightarrow y) = 1, P(x \rightarrow z) = 0 \text{ if } \text{Ham}(x \rightarrow z) > 1$$

Example: The only allowed neighbours for the 000 mode are {100, 010, 001}. All the other modes lie at hamming distance > 1 and have $P = 0$ (**Figure 1C**).

First-order dynamics arise as a primitive constraint: mass–energy cannot split across multiple discrete modes. Equivalently, axiom 3 can be derived from the physical separability of redox reaction events in space or time, each occurring sequentially and independently—with the Boolean hypercube emerging as a geometric corollary (**Supplemental Information**).

Axiom 4. Matter Curves the Modal Manifold

General relativity⁹ (GR) necessitates that the real physical mass-energy of an instantiated mode curves spacetime. By definition, that curvature belongs to the instantiated mode itself—a discrete object on the modal Boolean hypercube $\mathcal{M} = \{0,1\}^R$ per axiom 1.

Since modal transitions involve quantum mechanical processes like electron tunnelling¹⁴, the curvature of an instantiated proteoform object is modified by projecting it into the discrete, non-symplectic manifold (**Supplemental Information**). MGF Theory achieves this through a discrete projection functor, coupling what is real with what is abstract

$$\mathcal{F}: \mathcal{C}_{\text{REAL}} \rightarrow \mathcal{C}_{\text{ABSTRACT}}, \mathcal{F}(\rho)(x) = (L\rho)(x),$$

With modal scalar curvature

$$R(x) = (L\rho)(x), \sum_{x \in \mathcal{M}} R(x) = 0$$

The occupancy-induced local curvature modal manifold is inherited in discretised form from the real instantiation—itsself a discrete mode. Mathematical precedent in physics exists: wave amplitudes are transported into Hilbert space, thermodynamic ensembles into phase space, and gauge interactions into fibre bundles. In MGF Theory, proteoform occupancy curves the modal manifold (**Figure 1D**), constraining not what is, but what can be.

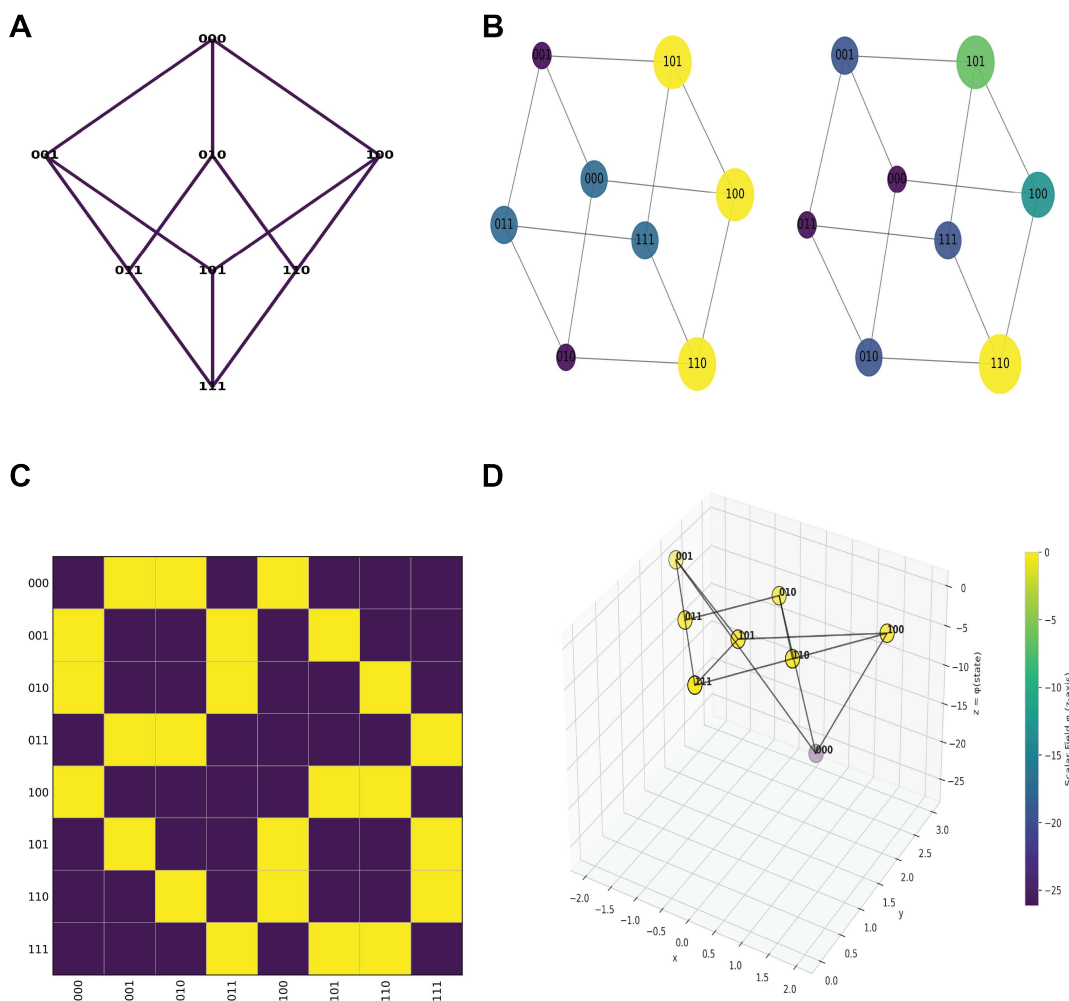


Figure 1. MGF Theory Axioms. A. Binomial theorem structured (1:3:3:1) Boolean lattice of proteoform modes in the combinatorics-enumerated $R=3$ series. B. The modal manifold is volume-invariant. No matter how molecules redistribute—depicted as a change in size of the nodes in left vs. right—the volume of the hypercube remains invariant. C. Adjacency matrix of allowed (yellow) and barred (purple) first-order modal transitions. D. Occupancy-induced—at “000”—induced deformation of the modal manifold, generates scalar Ricci curvature.

The MGF Theory Field Equation

The MGF Theory equation combines axioms 1-4 with energy and entropy:

$$\Delta f_{i \rightarrow k} = \underbrace{\Delta E_{i \rightarrow k} \cdot \exp [\rho(x_i) \cdot \Delta x_j]}_{\text{Energy}} - \underbrace{R(x_i)}_{\text{Curvature}} + \underbrace{\Delta S}_{\text{Entropy}}$$

- $\Delta f_{i \rightarrow k}$: Net driving potential for the transition $x_i \rightarrow x_k$.
- $\Delta E_{i \rightarrow k}$: Free energy cost or gain of the event (e.g., redox reaction).
- $\rho(x_i)$: Local occupancy at mode x_i . Encodes volume invariance by normalisation.
- Δx_j : Bitwise first-order transition step (Hamming-1), enforcing axiom 3.
- $R(x_i)$: Discrete Ricci curvature at mode x_i per axiom 4. Acts as a curvature penalty, resisting transitions against local geometric imbalance.
- ΔS : Entropy from heat, conformational changes, disorder, or degeneracy.

To enforce the conservation of probability across \mathcal{M} , one can impose the stationary condition:

$$\sum_{k=0}^R P(i \rightarrow k) \cdot \Delta f_{i \rightarrow k} = 0$$

ensuring that transitions respect global volume invariance axiom 2 while admitting the local redistribution of curvature per axiom 4.

Axioms 1–3 define invariant structural geometric constraints: the Boolean hypercube enumerates modes, volume is conserved, and transitions are restricted to first-order moves. Axiom 4 introduces curvature as a mutable regulator: concentrated occupancy creates steep wells that suppress transitions, while distributed occupancy flattens the manifold and facilitates motion. This is analogous to how transporting distributed mass (multi-modal distribution) is easier than concentrated mass (unimodal distribution). This curvature is the discrete analogue of energy basins, projected lawfully from real proteoforms into \mathcal{M} . The field equation encodes a geometry of proteoform dynamics.

Modelling MGF Theory

To model the MGF equation, the stepwise action integral (\mathcal{A}) was defined as:

$$\mathcal{A} = \sum_{s=1}^S [\Delta S(s) + \lambda_R R(x_s)^2 + \lambda_A \|A(x_s)\|^2]$$

where ΔS is the entropy gain, $R(x_s)$ the local curvature, and $A(x_s)$ the anisotropy at mode x_s .

Per the methods, 10^3 synthetic priors—each consisting of 100 molecules randomly distributed across the $\mathcal{M} = \{0,1\}^3$ modal Boolean manifold—were evolved for 100 steps under the probabilistic action limited evolution engine (ALIVE) algorithm. The action integral was instantiated along each trajectory, with entropy, curvature, anisotropy, and degeneracy contributions computed at every step and accumulated across runs.

Regression analysis revealed that geometry shaped proteoform dynamics (**Figure 2A**). High curvature suppressed \mathcal{A} ($\beta = -1059.7$, $p < 1e-94$), whereas directional anisotropy strongly amplified it ($\beta = +2112.8$, $p < 1e-88$). Hence, modal geometry governs proteoform dynamics, constraining or promoting transitions depending on curvature and anisotropy.

A discrete Lie-like operator algebra over \mathcal{M} was developed. Each bitflip defined an operator M_i acting on a given mode $x \in \mathcal{M}$. The resultant algebra is non-abelian: some operators cannot commute. For example, 000 and 111 cannot directly commute per axiom 3.

Finite modal sequences can commute (**Figure 2B**). For example, the sequence $000 \rightarrow 100 \rightarrow 101 \rightarrow 111$ defines a communicative algebraic substructure. Communicative substructures define geodesics—the shortest pathlength between 000 and 111 (**Figure 2C**)—per:

$$|\text{Geodesics}_k| = k!$$

yielding six geodesics:

1. $000 \rightarrow 100 \rightarrow 101 \rightarrow 111$

2. 000 \rightarrow 100 \rightarrow 110 \rightarrow 111
3. 000 \rightarrow 010 \rightarrow 011 \rightarrow 111
4. 000 \rightarrow 010 \rightarrow 110 \rightarrow 111
5. 000 \rightarrow 001 \rightarrow 101 \rightarrow 111
6. 000 \rightarrow 001 \rightarrow 011 \rightarrow 111

In the simulations, curvature introduced path-dependence across geodesics. Distinct geodesics connecting the same start (000) and end (111) mode produced asymmetric operator orderings (**Figure 2D**). Curvature enforced a non-abelian structure: operations that commute within a geodesic became non-commutative across geodesics. Proteoform dynamics can exhibit path-dependent hysteresis¹⁵.

The nested, recursive self-similar structure of the geodesics (**Figure 2E**) maps to the Sierpiński triangle when Pascal’s triangle is reduced modulo 2¹⁶. While these fractal-like structures evoke order and chaos^{17,18}, they take on a different meaning in a discrete, volume-invariant manifold. Axiom 1 bounds every Lyapunov exponent^{19,20}. In MGF Theory, Ricci Flow²¹

$$\Phi(\rho) = \max_{x, y, \in \mathcal{M}} |R(x; \rho) - R(y; \rho)|$$

behaves as a simple harmonic oscillator generator of *order* \rightarrow *chaos* \rightarrow *order*. At the left extreme, the system is maximally ordered. Local curvature is concentrated by all of the molecules occupy one mode (agnostic of mode identity). At the bottom, the system is maximally chaotic. Local curvature is dispersed evenly across all of the modes. No curvature-induced *order* weights modal transitions. Like a thermal system at equilibrium, they are all iso-potential. At the right extreme, the system is reordered—local curvature is reconcentrated by unimodal occupancy.

Modal dynamics span the full oscillator spectrum, admitting different frequencies of cycling between order and chaos. In this view, entropy is the inevitable, direction-agnostic product of curvature spread, quantified by

$$\Phi(\rho) = \sum_{x \in \mathcal{M}} \left(\rho_x - \frac{1}{|\mathcal{M}|} \right)^2$$

Where ρ_x is the normalised occupancy distribution. The bounded evolution of Ricci Flow admits a natural wave mechanic interpretation

- **Amplitude:** defined by modal degeneracy $D(t)$, bounded between one (all molecules in a single mode, maximum order) and R (uniform dispersion, maximum chaos).
- **Frequency:** determined by the periodicity of Ricci spread oscillations. Distinct trajectories generate different frequencies, reflecting asymmetry and geodesic trapping.
- **Phase:** set by operator ordering along geodesics. Non-commuting operator sequences introduce phase shifts, encoding path-dependence.

Across the simulations, the Ricci Flow amplitude of the ensemble trajectories showed that $D(t)$ fluctuates within this strict bound, oscillating between lower-degeneracy ordered states and higher-degeneracy chaotic states (**Figure 2F**). The black mean curve demonstrates the

emergent wave-like behaviour of degeneracy, with trajectories distributed around it within one standard deviation.

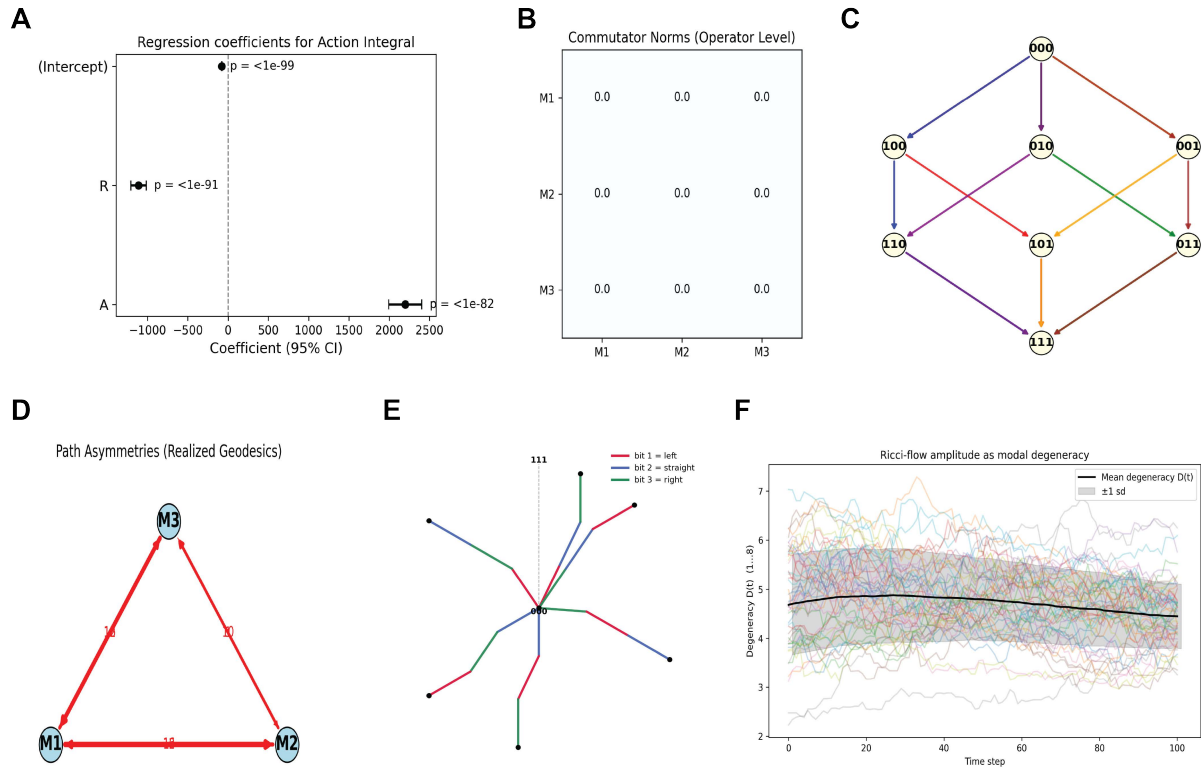


Figure 2. Modal Geometry Governs Proteoform Dynamics. **A.** Forest plot of regression coefficients (β , 95% CI) from general linear modelling of the action integral against mean curvature (R) and anisotropy (A). **B.** Heatmap of commutator norms between the empirical generators M1,M2,M3, where the numbers map to each cysteine bit. All values are near zero, consistent with symmetric operator action between allowed modes. **C.** Geodesics on the Boolean manifold. **D.** Directed graph of observed path motifs. Node size denotes operator identity, arrow thickness encodes motif frequency, and red arrows highlight asymmetries where $M_i \rightarrow M_j \neq M_j \rightarrow M_i$. Asymmetry represents non-commutativity geodesic orderings, even when the operator algebra appears symmetric as in panel C. **E.** Symbolic representation of the self-similar geodesics. From 000 radiating to 111, oxidation of bit 1, 2 and 3 deviates the trajectory of the line to the left, centre, and right, respectively. **F.** Ricci-flow amplitude across the simulated trajectories, the black line shows the mean degeneracy, one standard deviation is shown in grey.

Selected trajectories were selected projected into the complex domain as an example of discrete Mandelbrot-like²² shapes (**Figure 3**). Symmetric trajectories remained on the geodesic (trap fraction ≈ 0.97 , non-commutativity = 0), producing ordered Ricci waves with narrow spectra and nearly holomorphic complex orbits. Trapped trajectories deviate (trap fraction ≈ 0.73 , noncommutativity = 0.5), yielding chaotic Ricci waves, broadband spectra, broken holomorphy, and asymmetric operator adjacency.

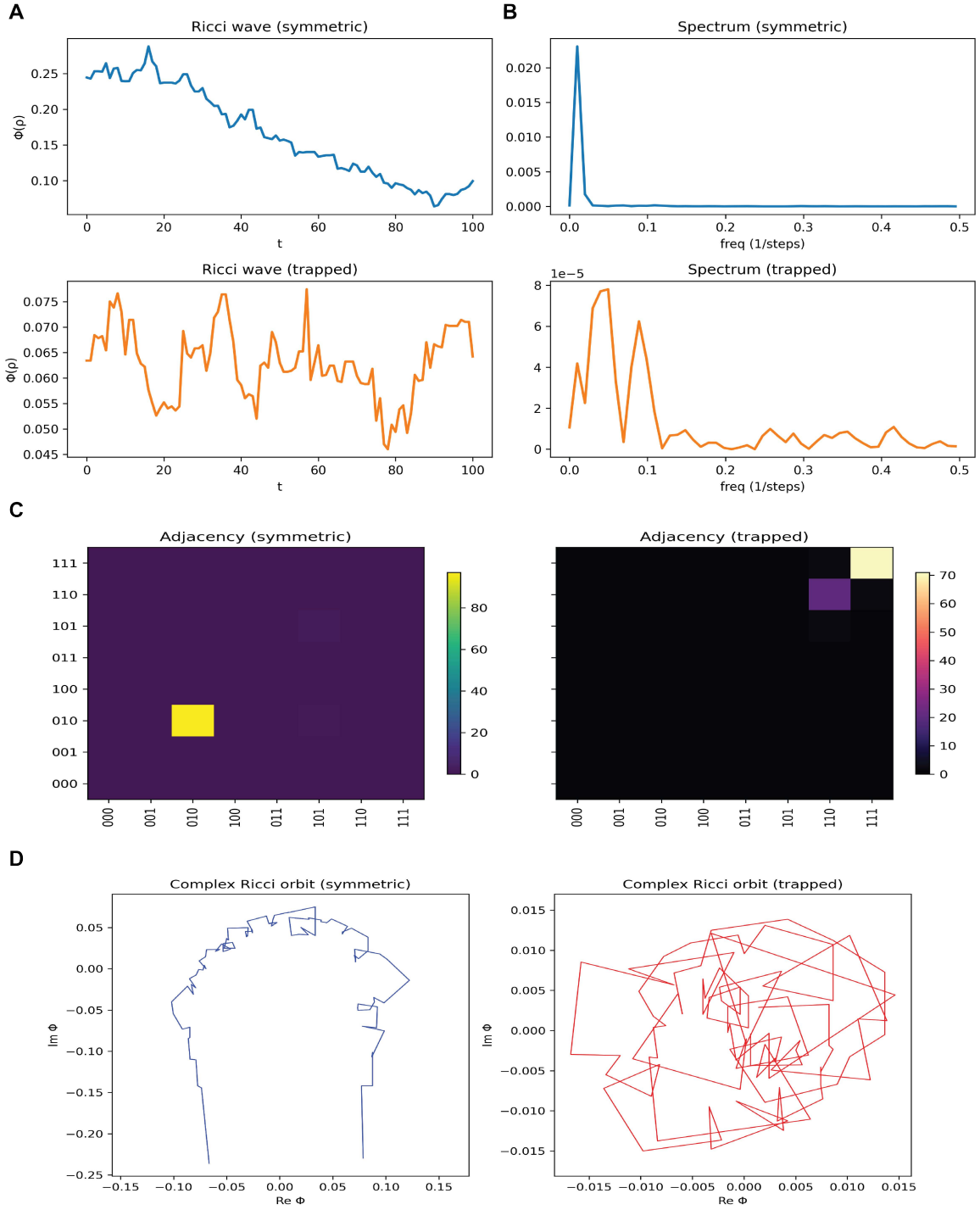


Figure 3. Ricci-wave dynamics reveal ordered vs trapped trajectories. A-B. Time series of Ricci spread $\Phi(\rho)$ and corresponding Fourier spectra for a representative symmetric trajectory (top) and a trapped trajectory (bottom). Symmetric dynamics exhibit smooth oscillations with narrow spectral content, whereas trapped dynamics show irregular fluctuations and broadband spectral power. **C.** Transition adjacency matrices of the same trajectories. Symmetric flow produces a sparse, geodesic-aligned structure, while trapped flow shows asymmetric clustering of transitions, indicative of non-commutativity. **D.** Complex projection of Ricci-wave trajectories using the analytic signal. Symmetric trajectories form near-holomorphic orbits in the complex plane, while trapped trajectories generate irregular, non-holomorphic paths with broken symmetry.

Modelling the MGF Theory field equation demonstrated that the Boolean hypercube constrained trajectories, volume was conserved, and transitions followed first-order moves

(axioms 1–3). Curvature acted as a mutable regulator (axiom 4), with concentrated occupancy suppressing transitions and distributed occupancy facilitating motion. The resulting Ricci waves, spectra, and complex orbits demonstrate how curvature, energy, and entropy govern proteoform.

Conservation of Curvature

While Ricci Flow²¹ can smooth the collective curvature of multi-molecule occupancy distribution molecules in \mathcal{M} , curvature is conserved at the single-molecule level. Formally, for a single-molecule occupying mode x , curvature is defined as the Laplacian of occupancy

$$R(x) = \Delta\rho(x)$$

Direct enumeration across all eight modes in the $R = 3$ series, revealed that while curvature is nonzero at the occupied mode the total curvature is zero

$$\sum_{x \in \mathcal{M}} R(x) = 0$$

The globally “flat” \mathcal{M} is locally deformed by molecular occupancy. In analogy to Noether’s theorem²³, the volume-invariance of the discrete non-symplectic \mathcal{M} (axiom 2) guarantees a conservation of curvature law (axiom 4). Curvature cannot be created or destroyed—only transported between neighbouring modes.

Computational enumeration of all single-molecule modal placements and random occupancy distributions (**Figure 4**) yielded $\sum_x R(x) = 0$ within machine tolerance ($< 10^{-12}$). Hence, curvature is conserved.

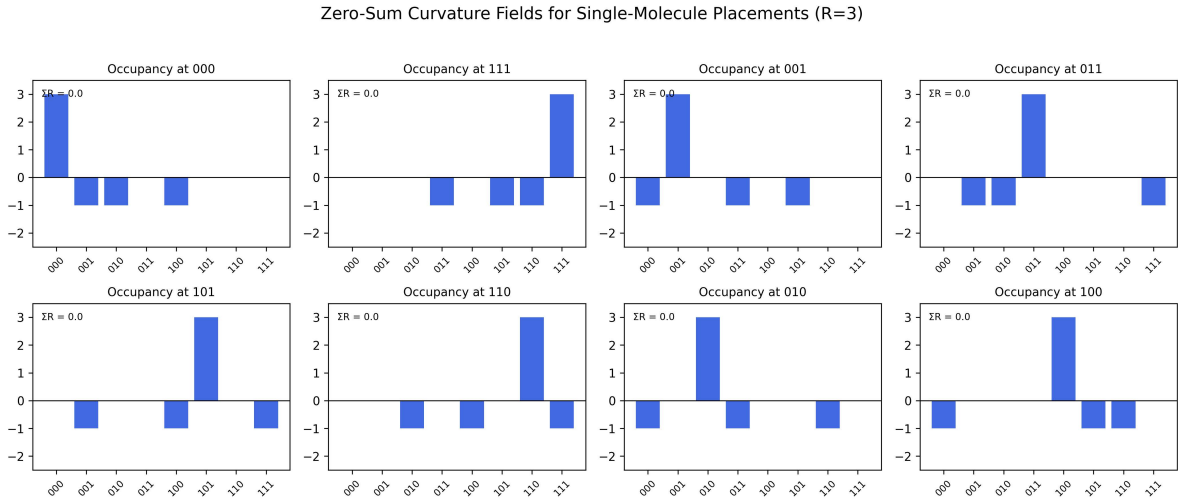


Figure 4. Conservation of curvature. The bar plot series showing the distribution of curvature across and the total curvature across each instantiated modal occupancy. In this case, the occupied node carries positive curvature (+3), its three Hamming-1 neighbours are compensated with (-1) curvature. Hence, despite the local deformation the global curvature is zero ($3 - 3 = 0$). The volume-invariant manifold, means that while curvature is mutable—it can be transported—the total curvature must be 0, establishing a discrete Noether-like analogue on the non-symplectic modal manifold.

The Geometric Primitive

A single-molecule instantiated in mode “000” must evolve to a valid neighbour (“100”, “010”, or “001”), if it is acted on or remain inert—establishing a discrete Einstein-Hilbert least-action analogue of axiom 3:

$$\mathcal{A} = \int R\sqrt{g} dv$$

If the “000” mode were acted upon, then “100”, “010”, and “001” are all iso-potential ($R(x) = -1$, **Figure 4**), and, therefore, equally probable ($P = 0.33$). The total curvature of the occupied mode (+3) is evenly partitioned across Hamming-1 neighbours because each bit is currently treated identically. Hence, nothing biases one allowed modal transition from another.

To differentiate otherwise iso-potential modal transitions, a Poisson partial differential equation (PDE) was solved on the atomic structure of human GAPDH ($R = 3$). For each cysteine bit, the PDE yielded a Dirichlet energy (E_b), and a local source energy (S_b), whose ratio defined a normalised bitwise projection weight (w_e). These values were functorially lifted into the modal Laplacian, yielding

- Cys152(bit1). $E_b = 2.42 \times 10^{-1}$, $S_b = 1.58 \times 10^{-1}$, $w_E = 0.388$
- Cys156 (bit2). $E_b = 2.11 \times 10^{-1}$, $S_b = 1.25 \times 10^{-1}$, $w_E = 0.351$
- Cys247(bit3). $E_b = 3.02 \times 10^{-1}$, $S_b = 1.32 \times 10^{-1}$, $w_E = 0.260$

By contrast persistent topological analysis of the local bitwise graph yielded nearly uniform Morse weights ($w_M \approx 0.333$), consistent with a symmetry-preserving background.

On the modal manifold, Dirichlet energies computed with the instantiated mode—source—fixed at “000” were:

- Energy-channel: $E = 4.62 \times 10^{-1}$
- Morse-channel: $E = 4.53 \times 10^{-1}$
- Fused (average): $E = 4.55 \times 10^{-1}$
- Fused (tropical): $E = 4.54 \times 10^{-1}$

Instantaneous outflow probabilities from a constrained Markov transition model under each channel further confirmed the PDE bias:

- Energy-channel: $\text{bit1} > \text{bit2} > \text{bit3}$
- Morse-channel: equal.
- Fused (average): $\text{bit1} > \text{bit2} > \text{bit3}$
- Fused (tropical): $\text{bit1} > \text{bit2} > \text{bit3}$

The tropical fusion implements the algebra of minimum action, selecting per bit the least-cost contribution between PDE curvature-energy and Morse topology. In this sense, it is a discrete instantiation of the Einstein-Hilbert variational principle on the modal manifold.

Time-evolution on the modal Laplacian confirmed that under the PDE-derived channel the “100” modal transition from “000” is consistently the geometric primitive. Biasing edge weights by the curvature of the PDE, revealed that bit3 had the greatest intrinsic curvature—consistent with resistance to action.

Functorial projection of PDE-derived curvature-energy into the modal manifold broke the degeneracy of iso-potential modal transitions, identifying $000 \rightarrow 100$ as the geometric primitive. This matches empirical evidence^{24–26}: Cys152 is experimentally verified as the most oxidation-prone cysteine²⁷. The model predicts that the “111” human GAPDH mode²⁸ arises via preferential action along the $000 \rightarrow 100 \rightarrow 110 \rightarrow 111$ geodesic. Beyond GAPDH, bitwise differentiation of the modal manifold provides a general method of identifying geometric primitives.

Curvature, Energy, and Entropy

Since the intrinsic curvature of the \mathcal{M} is invariant (axiom 4), a mode will remain inert—persisting indefinitely ($x_i \rightarrow \infty$) in the absence of forcing—per Newton’s first law. External energy (E), such as a redox reaction event^{29,30}, can pay the cost of transporting curvature from $x_i \rightarrow x_j$. Whether expressed as heat dissipation or configurational rearrangement, entropy (S) is an inseparable product of energy-coupled curvature transport per Ricci Flow, such that

$$E = x_i \rightarrow x_j + \Delta S, \quad S(x_i \rightarrow x_j) > 0$$

MGF Theory projects the real GR-derived curvature into the discrete \mathcal{M} to calculate

$$\Delta G = \kappa_{modal}|R(x)|,$$

where $R(x) = (L\rho)(x)$ is the scalar curvature induced by occupancy, and κ_{modal} is the geometric coupling constant. This relation states that curvature and energy are proportional, in exact analogy to GR, where curvature is tied to mass-energy via $G_{\mu\nu} = 8\pi T_{\mu\nu}$.

In this view, curvature becomes an energetic field property: any transport of modal curvature incurs a quantised energy cost—the activation energy³¹ (E_a) needed to transport modal curvature. Curvature transport only occurs when the necessary E_a is supplied. As energy is conserved, any surplus is partitioned into entropy and free energy (ΔG)

$$E_{IN} = E_a(x_i \rightarrow x_j) + \Delta S + \Delta G$$

Numerical example: For a GAPDH molecule instantiated in “000” the modal manifold, occupancy induced curvature produced a symmetric barrier height of $\approx 33 \text{ kJ} \cdot \text{mol}^{-1}$ per cysteine bit. By construction, this value is the same for all three bits, since the curvature spectrum is invariant under axiom 4.

Per the geometric primitive, the bitwise energy weights, calculated via the PDE solution of the real atomic structure, were used to differentiate the modal manifold

$$E_a(b) = \kappa_{modal}|K|(1 - \ln w_E(b))$$

where $|K|$ is the symmetric barrier height ($\approx 33 \text{ kJ} \cdot \text{mol}^{-1}$). Applied to Cys152, this equation yielded an activation energy of $76 \text{ kJ} \cdot \text{mol}^{-1}$, which is congruent with $67 \text{ kJ} \cdot \text{mol}^{-1}$ as computed from empirical kinetic data³² (see methods).

In MGF Theory, the mutability of curvature—it varies as occupancy changes—makes the activation energy relative. This idea lies at the centre of the field equation where the penalty

cost, such as the activation energy, of a modal transition decreases as Ricci Flow dissipates curvature.

Scale-invariance

MGF Theory is scale-invariant: it applies to any nonzero R integer. Adapting scripts to accommodate different R integers, revealed that the same axioms and equations applied across the scales. Regardless of how many modes compromise the manifold—its modal degrees of freedom, the laws acting on them remain the same.

Universality

Cysteine is no special case. MGF Theory generalises to any PTM on any amino acid (AA). Formally, the mathematics of an $R = 3$ \mathcal{M} are invariant, regardless of whether the three bits represented cysteine redox or tyrosine phosphorylation modes. For example, per axiom 1, there would be eight tyrosine phosphoforms modes: 000, 100, 010, 001, 110, 011, 101, and 111. Like the real to abstract categorical projection, AA-specified PTM morphisms of R can be described by a functor

$$\mathcal{F}: AA + PTM \rightarrow \mathcal{M}$$

The functor projects any AA-specified PTM-basis, from lysine acetylation to tryptophan oxidation, into the modal manifold. Under any functorial transformation, the axioms of MGF Theory remain invariant. Hence, MGF Theory is universal: It applies to all proteoforms, including every instantiated splice isoform and/or genetic variant.

Conclusion

MGF Theory explains how real and abstract modes are geometrically coupled through four axioms, uniting energy, entropy and curvature into a single framework. This formulation is consistent with thermodynamics and statistical mechanics, but crucially extends them geometrically. At this resolution, the globally “flat” modal manifold is locally deformed by occupancy, allowing iso-potential modes to be distinguished via geometric primitives. These primitives define least-action pathways that bias proteoform dynamics toward preferred geodesics, while still permitting alternative but geometrically lawful trajectories.

Methods

Source code

The [Julia](#)³³-scripted source code used to computationally instantiate the mathematics is available online at https://github.com/JamesCobley/Oxi_Shapes/tree/main.

Modelling the MGF Theory Field Equation

To model the MGF Theory field equation, the \mathcal{M} was initialised as a 2-dimensional diamond shaped—1:3:3:1—Boolean lattice graph, where the edges defined allowed—first-order—transitions between modes per axiom 1 and 3. To enforce axiom 2, the volume of the modal manifold as the probability of molecular distribution of the molecules was invariant:

$$\sum_x P(x) = 1$$

To enforce axiom 4, the $R(x)$ curvature was quantified as the local density imbalance in the \mathcal{M} , given by the graph Laplacian:

$$R(x) = \sum_{y \in N(x)} [\rho(y) - \rho(x)]$$

Where the $N(x)$ is the allowed neighbouring coordinates in the \mathcal{M} . To encode local geometric heterogeneity, each mode was treated as an anisotropic fibre bundle per:

$$A(x_i) = \frac{1}{|N(x_i)|} \sum_{x_j \in N(x_i)} \frac{|R(x_i) - R(x_j)|}{\|x_i^{(3D)} - x_j^{(3D)}\|}$$

- $x_i \in$ is a mode in the binomial lattice.
- $N(x_i)$ is neighbourhood of x_i , defined by a Hamming distance =1.
- $R(x)$ is the local scalar curvature at node x , computed as the discrete Laplacian of $\rho(x)$.
- $x_i^{(3D)} = (x_i^x, x_i^y, -\rho(x_i))$ are the 3D coordinates of x_i .
- $x_i^{(3D)} - x_j^{(3D)}$ is the Euclidean distance in the curved geometry.
- $A(x_i)$ is the anisotropy at node x_i , encoding local directional asymmetry in curvature.

These fibres are wrapped in a self-consistent sheath, representing the global volume invariant manifold. Modal transitions were then simulated per the field equation

$$\Delta f_{i \rightarrow k} = \underbrace{\Delta E_{i \rightarrow k} \cdot \exp[\rho(x_i) \cdot \Delta x_j]}_{Energy} - \underbrace{R(x_i)}_{Curvature} + \underbrace{\Delta S}_{Entropy}$$

The 10^3 modal occupancy distributions (ρ) were initialised from the random sampling of 100 molecules per run. The ALIVE algorithm stochastically updated occupancies across the \mathcal{M} using curvature-constrained Monte Carlo steps^{34,35}, with anisotropy acting as a directional penalty/weight. Given the biophysical constraints on energy-coupled redox reactions, the maximum number of moves permitted per step was set to ten. Each 100-step trajectory produced a time-series of $\rho(x)$, $R(x)$, and $A(x)$.

Action integral

To compute \mathcal{A} , entropy was quantified from symmetry degeneracy (S_{DEG}). Each mode at x with hamming weight k was weighted by the binomial degeneracy:

$$S_{DEG}(\rho) = \sum_i \rho(x_i) \log \frac{1}{\binom{R}{k}}$$

Where R is the residue integer and $\binom{R}{k}$ is the degeneracy of that oxidation integer (e.g., $k = 1$, degeneracy = 3). The cumulative \mathcal{A} along a trajectory was defined as the weighted sum of three contributions per time step:

$$\mathcal{A} = \sum_t \left[\alpha_{mass} \cdot \sum |\Delta \rho| + \alpha_{geom} \cdot (\langle R^2 \rangle + \langle \|A^2\| \rangle) + \alpha_{entropy} \cdot S_{deg}(\rho) \right]$$

Where $\Delta \rho$ is the flux, R the local curvature, and A the local anisotropy. The parameters ($\alpha_{mass}, \alpha_{geom}, \alpha_{entropy}$) were set to 0.01, 0.1, and 0.1, respectively. After computing \mathcal{A} along

all of the trajectories, statistical regression analysis was performed to determine the influence of curvature and anisotropy on action.

Discrete Algebra

A discrete operator algebra was constructed directly from the simulated proteoform trajectories. For each trajectory, stepwise transitions were parsed and encoded as triples (to,from, b), where b indexes the bit flipped. Each bit-flip thereby defined an operator M_b acting on \mathcal{M} . To build the empirical operators, sparse $N \times N$ matrices G_b were assembled such that

$$(G_b)_{ij} = P(x_i | x_j, b)$$

the conditional probability of reaching mode x_i from x_j via bitflip b , normalised with Laplace smoothing. The G_b series forms the empirical generators of the discrete algebra. Algebraic structure was quantified in two ways. First, for each operator pair, the commutator

$$[M_i, M_j] = M_i M_j - M_j M_i$$

was evaluated, and the Frobenius norm $\|[M_i, M_j]\|$ was computed. Vanishing norms indicated commutativity.

Second, path algebra was computed via parsing successive triplet transitions to count ordered pairs (M_i, M_j) . Asymmetries in counts between (M_i, M_j) and (M_j, M_i) indicated non-commutativity in practice—path-dependent operator orderings. Together, these analyses define a Lie-like discrete algebra over \mathcal{M} .

Ricci Flow

To analyse order and chaos in proteoform dynamics, each simulated trajectory was parsed into a time series of curvature values derived from occupancy $\rho(x)$ across the Boolean lattice \mathcal{M} per the graph Laplacian. The resultant Ricci functionals quantified how curvature was distributed across the lattice. Two equivalent forms were used

$$\Phi(\rho) = \max_{x, y, \in \mathcal{M}} |R(x; \rho) - R(y; \rho)|$$

And

$$\Phi(\rho) = \sum_{x \in \mathcal{M}} \left(\rho_x - \frac{1}{|\mathcal{M}|} \right)^2$$

The first form measures the maximal curvature contrast across the lattice; the second is a variance-like form showing deviation of the occupancy distribution from flatness. Both return zero for a uniform distribution (globally flat manifold) and increase as curvature concentrates.

To map the spectrum of behaviours between order and chaos Ricci Flow was defined as bounded modal degeneracy

$$D(t) = \frac{1}{\Phi(t) + 1/N} A(t) \frac{D(t) - 1}{N - 1}$$

where N is the total number of modes. By construction, $D(t)$ is bounded between 1 (all molecules in one mode; maximal order) and N (uniform distribution; maximal chaos). Hence, Ricci-flow dynamics can be expressed as a wave-like oscillation of degeneracy amplitude.

Bundles of $D(t)$ traces across replicate simulations were plotted to capture population-level dynamics. The ensemble mean and variance defined the central tendency and dispersion of degeneracy oscillations. To extract hidden oscillatory features, the Hilbert transform was applied to the ensemble-mean degeneracy trace, producing the analytic signal $z(t)$. From this, the oscillation envelope $|z(t)|$ (degeneracy amplitude) and the instantaneous frequency

$$v(t) = \frac{1}{2\pi} \frac{d}{dt} \arg(x(t))$$

were derived. These quantities provide a spectral decomposition of Ricci-flow dynamics, with amplitude representing excursions between ordered and chaotic states, frequency capturing the cycling periodicity, and phase reflecting operator ordering along geodesic.

To characterise the oscillatory geometry of selected trajectories, they were projected into the complex domain via the analytical signal. For the Ricci spread series $\Phi(t)$, the projection was computed as

$$z(t) = \text{Hilbert}(\Phi(t) - \langle \Phi \rangle)$$

where the Hilbert transform returns the analytic signal with real and imaginary components corresponding to the in-phase and quadrature parts of the oscillation. This maps each Ricci trajectory to a continuous orbit in the complex plane, allowing visualization of symmetric versus trapped dynamics.

Selected trajectories were reduced to its dominant state sequence, from which two algebraic metrics were computed:

1. **Geodesic trap fraction:** the proportion of the trajectory that lies within a canonical geodesic path.
2. **Non-commutativity score:** the fraction of observed two-step bit-flip sequences that are inconsistent with any canonical geodesic ordering.

These metrics distinguish between *symmetric* trajectories (high trap fraction, low noncommutativity) and *trapped* trajectories (low trap fraction, high noncommutativity). Complex projection of these examples produced qualitatively distinct orbits: symmetric trajectories formed near-holomorphic loops, while trapped trajectories generated irregular, non-holomorphic paths with phase discontinuities.

Conservation of Curvature

In the single-molecule basis, the Boolean lattice $\mathcal{M}\{0,1\}^R$ was realised as the Hamming-1 graph with symmetric adjacency W and Laplacian $L = D - W$. Curvature was defined as the discrete Laplacian $R = \Delta\rho = \Delta L$. Since $L^\top \mathbf{1} = 0$, total curvature vanishes for any occupancy

$$\sum_{x \in \mathcal{M}} R(x) = L^\top L\rho = 0,$$

Establishing a Noether-like discrete analogue: the volume-invariance of the \mathcal{M} per axiom 2 enforced a curvature conservation law, as confirmed by computational instantiation confirming machine-zero sums for all single-site placements and random $\rho(x)$.

The Geometric Primitive

Atomic coordinates were obtained from the AlphaFold¹ model of human [GAPDH](#) (AF-P04406-F1, v4). Cysteine residues were identified, and their C α coordinates extracted. Three cysteines (Cys152, Cys156, Cys247) were selected to define a 3-bit Boolean modal manifold ($R=3$).

To construct the substrate Laplacian, a weighted graph was constructed from all C α atoms using a Gaussian kernel with cut-off $r_c = 6.5 \text{ \AA}$ and width $\sigma 4.0 \text{ \AA}$. Edges between residues i, j were weighted as:

$$w_{ij} = \exp\left(-\frac{\|x_i - x_j\|^2}{2\sigma^2}\right), \|x_i - x_j\| \leq r_c$$

From the weighted adjacency W , the combinatorial Laplacian was computed as $L = D - W$, where is D the diagonal degree matrix.

To solve the PDE, each cysteine bit (b), a unit source term (ρ_b), was imposed at the C α coordinate, and the discrete Poisson equation was solved

$$L\phi_b = \rho_b - \langle \rho_b \rangle$$

Solutions ϕ_b were normalised to zero mean. The bitwise Dirichlet energy (E_b) and the local source energy (S_b) were computed as:

$$E_b = \frac{1}{2} \phi_b^\top L \phi_b, S_b = \frac{1}{2} \sum_j w_{bj} (\phi_b(b) - \phi_b(j))^2$$

The normalised pushforward weights were defined as

$$w_E b = \frac{S_b/E_b}{\sum_{\hat{b}} S_{\hat{b}}/E_{\hat{b}}}$$

To perform persistent topology analysis, local neighbourhoods of radius two edges were extracted from the substrate graph around each cysteine bit. Pairwise distances between neighbourhood residues were computed, and Vietoris–Rips filtrations applied to define two topological proxies:

- **H0 depth:** death time of the local cysteine bar (burial proxy).
- **H1 loopiness:** total persistence of finite H1 bars

Each proxy was normalised across bits, and combined as a morse-channel:

$$w_m b = \frac{depth_b / loop_b}{\sum_b (depth_b + Loop_b)}$$

The 3-bit modal manifold was represented as a Boolean hypercube, with the edges connecting Hamming-1 modes weighted according to their bitwise contributions. Multiple channel Laplacians were constructed: energy-only ($weights = w_E$), topology-only ($weights = w_M$), and a dual fused arithmetic mean ($(w_E + w_M)/2$) and tropical fusion, defined as:

$$w_{trop} b = \frac{\exp(-\min(-\log w_E(b), -\log w_M(b)))}{\sum_b \exp(-\min(-\log w_E(\hat{b}), -\log w_M(\hat{b})))}$$

Dirichlet energy of the resultant modal Laplacian was evaluated by solving

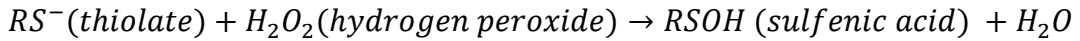
$$L_d \phi = \rho - \langle \rho \rangle, \rho = \delta 000$$

and computing $E = \frac{1}{2} \phi^\top L_d \phi$. Then instantaneous transition probabilities from “000” were calculated as normalised edge weights. A probabilistic propagation of the modal manifold, was simulated under the master-equation kernel/ The distributions at selected times were compared across the Laplacians.

Curvature of the substrate graph was approximated using Forman-Ricci curvature. For each cysteine, curvature was computed as the mean edge curvature of its neighbours, rescaled to $[0,1]$. Curvature values were fused functorially with PDE-derived weights to define curvature-fused modal Laplacians.

Numerical Example GAPDH Empirical

The rate constant (k) for the reaction



between Cys152 in GAPDH (2 μ M) and H₂O₂ (50 μ M) is $\approx 7M^{-1}s^{-1}$ at 20°C and pH 7.4, as calculated empirically³², was calculated as the Gibbs free energy (ΔG^\ddagger) activation energy per the Eyring³¹ equation

$$k = \kappa \frac{k_B T}{h} \frac{1}{C^\circ} \exp\left(-\frac{\Delta G^\ddagger}{RT}\right)$$

where k_B is the Boltzmann constant, h is Planck’s constant, T is temperature, $\kappa \approx 1$ is the transmission coefficient, and $C^\circ = 1M$ is the standard state concentration for bimolecular reactions. Rearranging,

$$\Delta G^\ddagger = -RT \ln\left(\frac{\kappa h C^\circ}{k k_B T}\right)$$

Substituting the empirical k at 293.15 K yielded $\Delta G^\ddagger \approx 67\text{ kJ mol}^{-1}$ (16 kcal mol⁻¹).

Curvature & Energy

To estimate the activation energy using MGF Theory, the modal manifold was initialised. Allowed Hamming-1 edges were weighted by occupancy differences, and Forman-Ricci curvature was computed on each edge. This produced a symmetric curvature spectrum: each bit-flip from “000” carried the same curvature-derived barrier height. To give this curvature physical units, the magnitude of modal curvature was mapped to energy by:

$$\Delta G_{curv}^{\ddagger} = \kappa_{modal} |K_{ij}|,$$

Where κ_{modal} is the geometric coupling constant ($J \cdot mol^{-1}$). This defines a baseline activation energy, that is symmetrical to each bit.

To differentiate this curvature bitwise, the real manifold projection weights $w_E(b)$ from the geometric primitive were applied as logarithmic scalars

$$\Delta G_{eff}^{\ddagger}(b) = \Delta G_{curv}^{\ddagger}(1 - \ln w_E(b))$$

This functorially lifts the PDE-derived heterogeneity into the modal manifold, producing differentiated barriers consistent with empirical kinetics. This approach preserves bitwise discriminatory power while inheriting physical units from the curvature–energy mapping.

Scale-invariance

To test scale-invariance, the source code used to implement the MGF Theory Field equation in the $R = 3$ basis was adapted to accommodate different R integers. The instantiated axioms and their evolution via the ALIVE algorithm remained invariant.

References

1. Jumper, J. *et al.* Highly accurate protein structure prediction with AlphaFold. *Nature* **596**, 583–589 (2021).
2. Smith, L. M. *et al.* Proteoform: a single term describing protein complexity. *Nat Methods* **10**, 186–187 (2013).
3. Smith, L. M. & Kelleher, N. L. Proteoforms as the next proteomics currency. *Science* **359**, 1106–1107 (2018).
4. Carbonara, K., Andonovski, M. & Coorssen, J. R. Proteomes Are of Proteoforms: Embracing the Complexity. *Proteomes* **9**, 38 (2021).
5. Burnum-Johnson, K. E. *et al.* New Views of Old Proteins: Clarifying the Enigmatic Proteome. *Mol Cell Proteomics* **21**, 100254 (2022).
6. Aebersold, R. *et al.* How many human proteoforms are there? *Nat Chem Biol* **14**, 206–214 (2018).
7. Cobley, J. N., Chatzinikolaou, P. N. & Schmidt, C. A. The Nonlinear Cysteine Redox Dynamics in the i-Space: A Proteoform-centric Theory of Redox Regulation. *Redox Biol.* 103523 (2025) doi:10.1016/j.redox.2025.103523.
8. Huang, K. *Statistical Mechanics*. vol. 2nd Edition (Wiley-VCH, 1987).
9. Einstein, A. Die Grundlage der allgemeinen Relativitätstheorie. *Ann Phys* **49**, 769–822 (1916).
10. Cobley, J. N. Oxiforms: Unique cysteine residue- and chemotype-specified chemical combinations can produce functionally-distinct proteoforms. *Bioessays* **45**, (2023).

11. Cobley, J. N. Exploring the unmapped cysteine redox proteoform landscape. *Am. J. Physiol.-Cell Physiol.* (2024) doi:10.1152/ajpcell.00152.2024.
12. Stanley, R. P. *Enumerative Combinatorics*. (2011). doi:10.1017/cbo9781139058520.
13. Parvez, S., Long, M. J. C., Poganik, J. R. & Aye, Y. Redox Signaling by Reactive Electrophiles and Oxidants. *Chem Rev* **118**, 8798–8888 (2018).
14. Moser, C. C., Keske, J. M., Warncke, K., Farid, R. S. & Dutton, P. L. Nature of biological electron transfer. *Nature* **355**, 796–802 (1992).
15. Cobley, J. N. Information, Geometry, and Chaos: Revealing Latent Cysteine Butterflies on Fractal Redox Shapes in the Proteomic Spectra. *Preprints* doi:10.20944/preprints202507.2120.v1.
16. Bannink, T. & Buhman, H. Quantum Pascal's Triangle and Sierpinski's carpet. *arXiv* (2017) doi:10.48550/arxiv.1708.07429.
17. Choudhary, D., Foster, K. R. & Uphoff, S. Chaos in a bacterial stress response. *Curr. Biol.* **33**, 5404-5414.e9 (2023).
18. Gleick, J. *Chaos: Making the New Science*. (Penguin Books, 2008).
19. LYAPUNOV, A. M. The general problem of the stability of motion. *Int. J. Control* **55**, 531–534 (1992).
20. Wolf, A., Swift, J. B., Swinney, H. L. & Vastano, J. A. Determining Lyapunov exponents from a time series. *Phys. D: Nonlinear Phenom.* **16**, 285–317 (1985).
21. Perelman, G. The entropy formula for the Ricci flow and its geometric applications. *arXiv* (2002) doi:10.48550/arxiv.math/0211159.
22. Mandelbrot, B. B. Fractals in physics: Squig clusters, diffusions, fractal measures, and the unicity of fractal dimensionality. *J. Stat. Phys.* **34**, 895–930 (1984).
23. Noether, E. & Tavel, M. A. Invariant Variation Problems. *arXiv* (2005) doi:10.48550/arxiv.physics/0503066.
24. Glover, M. R., Davies, M. J. & Fuentes-Lemus, E. Oxidation of the active site cysteine residue of glyceraldehyde-3-phosphate dehydrogenase to the hyper-oxidized sulfonic acid form is favored under crowded conditions. *Free Radic. Biol. Med.* (2023) doi:10.1016/j.freeradbiomed.2023.12.015.
25. Talwar, D. *et al.* The GAPDH redox switch safeguards reductive capacity and enables survival of stressed tumour cells. *Nat Metabolism* 1–17 (2023) doi:10.1038/s42255-023-00781-3.
26. Ralser, M. *et al.* Dynamic rerouting of the carbohydrate flux is key to counteracting oxidative stress. *J Biology* **6**, 10 (2007).
27. Peralta, D. *et al.* A proton relay enhances H₂O₂ sensitivity of GAPDH to facilitate metabolic adaptation. *Nat Chem Biol* **11**, 156–163 (2015).
28. Montfort, C. von *et al.* The role of GAPDH in the selective toxicity of CNP in melanoma cells. *PLOS ONE* **19**, e0300718 (2024).
29. Brown, G. C. Bioenergetic myths of energy transduction in eukaryotic cells. *Front. Mol. Biosci.* **11**, 1402910 (2024).
30. Cobley, J. N. 50 shades of oxidative stress: A state-specific cysteine redox pattern hypothesis. *Redox Biol.* **67**, 102936 (2023).
31. Eyring, H. The Activated Complex in Chemical Reactions. *J. Chem. Phys.* **3**, 107–115 (1935).
32. Winterbourn, C. C., Peskin, A. V., Kleffmann, T., Radi, R. & Pace, P. E. Carbon dioxide/bicarbonate is required for sensitive inactivation of mammalian glyceraldehyde-3-phosphate dehydrogenase by hydrogen peroxide. *Proc National Acad Sci* **120**, e2221047120 (2023).
33. Roesch, E. *et al.* Julia for biologists. *Nat Methods* 1–10 (2023) doi:10.1038/s41592-023-01832-z.

34. Metropolis, N. & Ulam, S. The Monte Carlo Method. *J. Am. Stat. Assoc.* **44**, 335–341 (1949).
35. Kalos, M. H. & Whitlock, P. A. Monte Carlo Methods. (2022)
doi:10.1002/9783527626212.

Supplemental Information

Axiom 1 Extended to Multinomial Theorem.

The structure of the entire proteoform state space (Ω_P)—all theoretically possible molecular variants from a single copy of a [UniProt](#) accession or proteome comprising multiples thereof—can be derived from multinomial theorem:

$$|\Omega_P| = \sum_{PS=1}^{N_{PS}} (19^{L_{PS}} \times M_{PS})$$

Where:

- N_{PS} is the number of protein species (PS) inclusive of frameshifts, splice variants, and indels.
- $\sum_{PS=1}^{N_{PS}} i$ is the sum for each PS.
- $19^{L_{PS}}$ is the genetic mutation state space for each AA, which can be mutated 19 ways from the original, for the PS, which can have different L due to indels.
- $M_{PS} = \prod_{i=1}^{L_{PS}} n_{i,PS}$ is the post-translational modification (PTM) state space for each AA in the PS, where $n_{i,PS}$ is the total number of PTM states (including unmodified) at residue i .

For example, a set comprising 10 PS with $L = 100$ where AA could be modified in at least one way, results in: $|\Omega_P| = 1.26 \times 10^{31}$ unique proteoforms. modes.

Multinomial theorem hierarchically organises this space Pascal Simplex (\mathfrak{H}_P). Within \mathfrak{H}_P , each proteoform occupies a unique coordinate in a multidimensional structure with two key planes:

1. **Horizontal Plane** – Encodes PTM state-space structure using multinomial coefficients, stratifying proteoforms by their modification-level degeneracy.
2. **Vertical Plane** – Encodes sequence-level divergence, placing near-identical PS (e.g., isoforms or mutations) closer together.

This multinomial Pascal simplex that structures the entire proteoform landscape across sequence variability and PTM states. All proteoform modes—whether arising from mutations, splicing, or PTMs—exist within a unified, mathematically constrained geometry. For example, GAPDH ($L = 335$) exists within a multinomial coefficient space where its 111-cysteine mode is just one of 6,209,895 possible modes within the k -3 modification-stratified ensemble (0.89%-PTM-speciated) of 336- k -states.

This simplex demonstrates how combinatorics-enumerated modal state spaces can naturally be extended to accommodate different PTM types, such as sulfenic acids, disulfide bonds, and thiyl radicals in the cysteine basis.

Axiom 2 Volume Invariance.

On the modal Boolean manifold $X = \{0,1\}^R$ occupancy is described by a probability distribution $\rho_t(x)$. Conservation of total mass requires

$$\sum_{x \in \mathcal{M}} \rho_t(x) = \sum_{x \in \mathcal{M}} \rho_{t+1}(x) = 1$$

For a discrete update rule. Let $P_t(x \rightarrow y)$ be the probability of mode transition from x to y . Then

$$\rho_{t+1}(y) = \sum_{x \in \mathcal{M}} \rho_t(x) P_t(x \rightarrow y)$$

Conservation of probability holds if

$$\sum_{y \in X} P_t(x \rightarrow y) = 1 \quad \forall x \in X$$

That is, P_t is a stochastic matrix. To define the continuity equation in flux form. Let $J_t(x \rightarrow y) = \rho_t(x) P_t(x \rightarrow y)$ then

$$\rho_{t+1}(x) - \rho_t(x) = \sum_{y \in N(x)} [J_t(y \rightarrow x) - J_t(x \rightarrow y)]$$

where $N(x)$ are the Hamming-1 neighbours of x . Summing over all x cancels fluxes and guarantees conservation.

In continuous time series with transition rates $k_{xy} \geq 0$

$$\dot{\rho}(x) = \sum_{y \in N(x)} [\rho(y)k_{yx} - \rho(x)k_{xy}]$$

with $\sum_x \dot{\rho}(x) = 0$. This is the discrete, non-symplectic analogue of Liouville's theorem.

The dynamic synthesis and degradation of instantiated molecules is accommodated by the source term $s_t(x)$

$$\rho_{t+1}(x) - \rho_t(x) = \sum_{y \in N(x)} [J_t(y \rightarrow x) - J_t(x \rightarrow y)] + s_t(x)$$

With total occupancy

$$N_{t+1} = \sum_x \rho_{t+1}(x) = N_t + \sum_x s_t(x)$$

One obtains

$$\rho_{t+1}(y) = \sum_x \rho_t(x) P_t(x \rightarrow y)$$

Since both numerator and denominator scale with N_t , the stochastic P_t kernel remains invariant regardless of the total occupancy of the \mathcal{M} , and the normalised probability distribution continues to satisfy $\sum_x \rho_t(x) = 1$.

Axiom 3 First Order Dynamics from Physics.

If time or space is fundamental, then each reaction corresponds to a distinct event that must be localised either temporally or spatially. Such events cannot be perfectly simultaneous. Special relativity demonstrates that absolute simultaneity is undefined: the temporal order of events depends on the frame of reference. At the molecular scale, this means that what appears as a “two-site jump” is not a primitive transition but rather the composition of two sequential first-order events, however, finely separated in time or space.

This principle is entirely consistent with calculus: continuous processes are understood as limits of infinitesimal increments. On a discrete manifold, the analogue is that multi-site modal changes ($\Delta k > 1$) necessarily decompose into sequential first-order transitions along the Boolean edges of the modal hypercube.

Geometric corollary: Formally, $\mathcal{M} = \{0,1\}^R$ is the R -dimensional Boolean hypercube, with vertices corresponding to modes and edges corresponding to single-site transitions. This can be represented as a binomial diamond, by stratifying modes according to Hamming weight (k). This projection preserves the combinatorial structure relevant to modal dynamics.

Axiom 4 Matter Curves the Modal Manifold.

On the Boolean hypercube $\mathcal{M} = \{0,1\}^R$, the discrete Laplacian is defined as:

$$(L\rho)(x) = \sum_{y \in N(x)} [\rho(y) - \rho(x)],$$

Where $N(x)$ are the Hamming-1 neighbours of mode x . This ensures

$$\sum_{x \in \mathcal{M}} (L\rho)(x) = 0$$

which enforces axiom 2 while allowing local curvature per axiom 4.

The functorial projection of real curvature onto the modal manifold is not arbitrary. In GR, curvature resides in the real manifold (spacetime). In MGF Theory, the functor transports this real curvature to the modal manifold. This mirrors other canonical functorial transports in physics like wave amplitudes into Hilbert space.

What MGF adds is a higher-order understanding: proteoforms, as classical objects undergoing quantum events, induce real curvature that cannot be fully described in spacetime alone. The modal manifold is a lawful abstract substrate onto which this curvature is projected, making accessible a space where one can compute dynamics of what *can be*, not only what *is*. Hence, the modal manifold is not an arbitrary construction but a framework for understanding known physics when applied to complex molecular systems.